nature genetics

Loss-of-function mutations in *MGME1* impair mtDNA replication and cause multisystemic mitochondrial disease

Cornelia Kornblum[1,13], Thomas J Nicholls[2,13], Tobias B Haack[3,13], Susanne Schöler[4,5], Viktoriya Peeva[4,5], Katharina Danhauser[3], Kerstin Hallmann[4,5], Gábor Zsurka[4,5], Joanna Rorbach[2], Arcangela Iuso[3], Thomas Wieland[3], Monica Sciacco[6], Dario Ronchi[7], Giacomo P Comi[7], Maurizio Moggio[6], Catarina M Quinzii[8], Salvatore DiMauro[8], Sarah E Calvo[9–11], Vamsi K Mootha[9–11], Thomas Klopstock[12], Tim M Strom[3], Thomas Meitinger[3], Michal Minczuk[2], Wolfram S Kunz[4,5] & Holger Prokisch[3]

Known disease mechanisms in mitochondrial DNA (mtDNA) maintenance disorders alter either the mitochondrial replication machinery (*POLG*, *POLG2* and *C10orf2*)[1–3] or the biosynthesis pathways of deoxyribonucleoside 5′-triphosphates for mtDNA synthesis[4–11]. However, in many of these disorders, the underlying genetic defect has yet to be discovered. Here, we identify homozygous nonsense and missense mutations in the orphan gene *C20orf72* in three families with a mitochondrial syndrome characterized by external ophthalmoplegia, emaciation and respiratory failure. Muscle biopsies showed mtDNA depletion and multiple mtDNA deletions. *C20orf72*, hereafter *MGME1* (mitochondrial genome maintenance exonuclease 1), encodes a mitochondrial RecB-type exonuclease belonging to the PD–(D/E)XK nuclease superfamily. We show that MGME1 cleaves single-stranded DNA and processes DNA flap substrates. Fibroblasts from affected individuals do not repopulate after chemically induced mtDNA depletion. They also accumulate intermediates of stalled replication and show increased levels of 7S DNA, as do MGME1-depleted cells. Thus, we show that MGME1-mediated mtDNA processing is essential for mitochondrial genome maintenance.

At present, only three nuclear genes directly involved in mtDNA replication have been associated with mitochondrial disease[1–3]. Pathogenic mutations in these genes result in two molecular phenotypes, multiple mtDNA deletions (multiple mtDNA deletion disorders) and/or reduction of mtDNA copy number (mtDNA depletion syndromes, MDS). Multiple mtDNA deletion disorders and MDS are clinically and genetically overlapping entities, known collectively as mtDNA maintenance disorders. Their clinical manifestations range from severe multiorgan involvement in early childhood to tissue-specific manifestations, for example, myopathies, in late adulthood. Progressive external ophthalmoplegia (PEO) is commonly associated with these disorders, particularly the late-onset phenotypes.

We identified a Lebanese family (family I) with three children affected by a severe multisystemic mitochondrial disorder (**Supplementary Fig. 1a**). Initial symptoms included ptosis in childhood followed by mild PEO, diffuse skeletal muscle wasting and weakness, profound emaciation and respiratory distress. Skeletal muscle biopsies showed scattered cytochrome c oxidase (COX)-negative fibers and ragged red fibers (RRFs) in all affected individuals. Respiratory chain enzyme activities were decreased in skeletal muscle (**Supplementary Table 1**). Mutations in mtDNA and nuclear genes associated with PEO were excluded by Sanger sequencing. To find the underlying genetic cause, we captured the exome of subject P1976 and performed massively parallel sequencing[12]. We applied several filtering steps, excluding intronic variants at non-canonical splice sites, synonymous variants and variants present in 816 exomes from individuals with unrelated diseases (**Supplementary Table 2**). Assuming an autosomal recessive mode of inheritance and focusing on genes predicted to encode mitochondrial proteins[13], this approach selected two genes, *SPTLC3* and *C20orf72*. Unlike *SPTLC3*, *C20orf72* harbored a homozygous nonsense mutation (c.456G>A, p.Trp152*) that was present in all affected subjects but not in healthy siblings, and both parents were heterozygous carriers (**Supplementary Fig. 1a**).

In parallel, we applied targeted MitoExome sequencing[14,15] and identified two additional affected individuals in an Italian family (family II) with the same homozygous nonsense mutation in *C20orf72* (**Supplementary Fig. 1b**). Haplotype analysis identified

[1]Department of Neurology, University of Bonn Medical Center, Bonn, Germany. [2]Medical Research Council (MRC) Mitochondrial Biology Unit, Cambridge, UK. [3]Institute of Human Genetics, Technische Universität München and Helmholtz Zentrum München–German Research Center for Environmental Health, Munich, Germany. [4]Department of Epileptology, University of Bonn Medical Center, Bonn, Germany. [5]Life and Brain Center, University of Bonn Medical Center, Bonn, Germany. [6]Neuromuscular Unit, Fondazione Istituto di Ricovero e Cura a Carattere Scientifico (IRCCS) Ca' Granda, Ospedale Maggiore Policlinico, Centro Dino Ferrari, University of Milan, Milan, Italy. [7]Neurology Unit, Fondazione IRCCS Ca' Granda, Ospedale Maggiore Policlinico, Centro Dino Ferrari, University of Milan, Milan, Italy. [8]Department of Neurology, Columbia University Medical Center, New York, New York, USA. [9]Department of Molecular Biology and Medicine, Massachusetts General Hospital, Boston, Massachusetts, USA. [10]Department of Systems Biology, Harvard Medical School, Boston, Massachusetts, USA. [11]Broad Institute, Cambridge, Massachusetts, USA. [12]Department of Neurology, Friedrich-Baur-Institute, Ludwig-Maximilians-Universität München, Munich, Germany. [13]These authors contributed equally to this work. Correspondence should be addressed to M. Minczuk (michal.minczuk@mrc-mbu.cam.ac.uk) or W.S.K. (wolfram.kunz@ukb.uni-bonn.de).

Received 7 August 2012; accepted 28 November 2012; published online 13 January 2013; doi:10.1038/ng.2501

Table 1 Clinical overview of individuals with *MGME1* mutations

	Family I (Lebanese)			Family II (Italian)		Sporadic case (German)
	P1976	P2061	P3737	P4050	P4052	P931
Sex	Male	Female	Male	Male	Male	Female
Age at first visit (years)	10	17	~14	31	36	35
Current age (years)	26	33	Death at 26 (cardiac failure)	53	42	Death at 73 (respiratory failure)
MGME1 mutation	c.456G>A (p.Trp152*)	c.456G>A (p.Trp152*)	c.456G>A (p.Trp152*)	c.456G>A (p.Trp152*)	c.456G>A (p.Trp152*)	c.698A>G (p.Tyr233Cys)
Clinical phenotype (major clinical findings)	PEO with proximal weakness and generalized muscle wasting, profound emaciation, respiratory failure (non-invasive ventilation)		PEO with exercise intolerance and generalized muscle wasting, profound emaciation, dyspnea	PEO with proximal weakness and generalized muscle wasting, profound emaciation, respiratory failure (non-invasive ventilation)		PEO with proximal weakness, respiratory failure (non-invasive ventilation), emaciation in advanced stage
BMI	11.8	12.7	12.3	NA	17.1	NA
Secondary clinical symptoms	Mental retardation, gastrointestinal symptoms, renal colics, spinal deformities	Mental retardation, gastrointestinal symptoms, spinal deformities, mild ataxia	Mental retardation, gastrointestinal symptoms, spinal deformities, dilated cardiomyopathy	Mild spinal deformities	Renal colics, mild spinal deformities	Cardiac arrhythmias, depressive episodes, memory deficits
Brain imaging (age in years)	Cerebellar atrophy on MRI and cranial CT scan (10 and 26)	Cerebellar atrophy on MRI (17)	Cerebellar atrophy on MRI (23)	NA		Mild cerebral atrophy on cranial CT scan (57)
Skeletal muscle biopsy (age in years)	Vastus lateralis (10): few RRFs, few scattered COX-negative fibers, 0.4%	Biceps brachii (17): RRF, few scattered COX-negative fibers, 0.6%	Vastus lateralis (23): RRF, scattered COX-negative fibers, 6.2%	Biceps brachii (31): few RRFs, scattered COX-negative fibers, 1.4–1.7%	Biceps brachii (37), triceps brachii (41): few RRFs, scattered COX-negative fibers, 1.5%, 2%	Vastus lateralis (57): RRF, scattered COX-negative fibers, 3.6%
Respiratory chain enzyme activities	Combined complex I/IV deficiency		Complex I deficiency	Normal	Combined complex I/IV deficiency	NA
Long-range PCR	multiple mitochondrial DNA deletions (present in all muscle biopsies)					
NMDAS (0–145 points)	48 points (age 26)	37 points (age 33)		NA		

BMI, body mass index; CT, computed tomography; MRI, magnetic resonance imaging; RRF, ragged red fibers; COX, cytochrome c oxidase; NA, not available; NMDAS, Newcastle Mitochondrial Disability Adult Scale (higher scores indicate more severe disease).

a homozygous region of 1.1 Mb shared by both families, suggesting that the mutation derives from a common founder (**Supplementary Table 3**). In addition, we identified a homozygous c.698A>G (p.Tyr233Cys) mutation in a sporadic case from Germany. All subjects with *C20orf72* mutations presented with markedly similar clinical and histological phenotypes (**Table 1**, **Supplementary Fig. 2** and **Supplementary Note**).

Analysis of the primary structure of the protein encoded by *C20orf72*, renamed *MGME1*, showed that it belongs to the PD–(D/E)XK nuclease superfamily[16], a large and diverse group of enzymes having various nucleic acid cleavage activities. In addition to the principal PD–(D/E)XK motifs I, II and III (**Fig. 1a**, green, yellow and blue, respectively), MGME1 contains a QhXXY motif, where h represents a hydrophobic residue and X represents any residue, characteristic of the RecB-type family[17] (**Fig. 1a**, red). Three-dimensional homology modeling of the MGME1 active site based on the crystal structure of *Escherichia coli* RecB[18] indicated a very similar arrangement of the key catalytic residues (**Fig. 1b**). The c.456G>A (p.Trp152*) mutation occurs upstream of the PD–(D/E)XK nuclease motif, such that the truncated product is very likely to not be functional. Even so, we did not observe any detectable levels of either full-length or truncated MGME1 in fibroblasts from subject P1976 (**Fig. 1c**), with the latter result most likely owing to nonsense-mediated mRNA decay. The c.698A>G (p.Tyr233Cys) mutation found in the sporadic case affects a conserved amino-acid residue (**Fig. 1a**). MGME1 contains a predicted N-terminal mitochondrial targeting signal, and immunohistochemical subcellular localization of green fluorescent protein (GFP)-tagged MGME1 in human fibroblasts (**Fig. 1d**) and cell fractionation (**Supplementary Fig. 3**) showed that MGME1 localizes to the mitochondria.

To clarify the molecular consequences of the *MGME1* mutations, we analyzed available tissue samples for the presence of mtDNA deletions or mtDNA depletion. Long-range PCR showed the presence of multiple mtDNA deletions in the muscle biopsies from all affected individuals and in the blood and urine samples of family I (**Supplementary Fig. 4**). The deletions were unusually large in comparison to those observed in individuals with *POLG* mutations. Quantitative assessment of deletions by single-molecule PCR revealed total deletion loads between 0.04% and 1.5% in skeletal muscle (**Supplementary Table 4**), which is similar to the levels observed in individuals with *POLG* mutations (**Supplementary Table 4**). mtDNA copy-number analysis detected substantial mtDNA depletion in all affected adults (P2061, P3737, P4050, P4052 and P931) (**Fig. 2a**). Only the muscle biopsy from subject P1976, which was taken when he was 10 years old and only mildly symptomatic, had normal mtDNA copy numbers. The finding of mtDNA depletion and mtDNA deletions in skeletal muscle from individuals with *MGME1* mutations suggested perturbed mtDNA maintenance as the primary cause of the mitochondrial disease in these individuals.

In addition to mtDNA depletion, we observed a relative increase in 7S DNA levels. 7S DNA is the single-stranded component of the mtDNA displacement loop (D loop) and is postulated to be an intermediate of prematurely terminated mtDNA replication. The ratios of 7S mtDNA to total mtDNA were twofold to eightfold higher compared to controls in five of the six investigated muscle tissues (**Fig. 2a**) and the fibroblasts from subject P1976 (**Fig. 2b**). This phenomenon was also observed in cells subjected to small interfering RNA (siRNA) downregulation of *MGME1* (**Fig. 2b** and **Supplementary Fig. 5a**), suggesting a direct involvement of MGME1 in the turnover of 7S DNA.

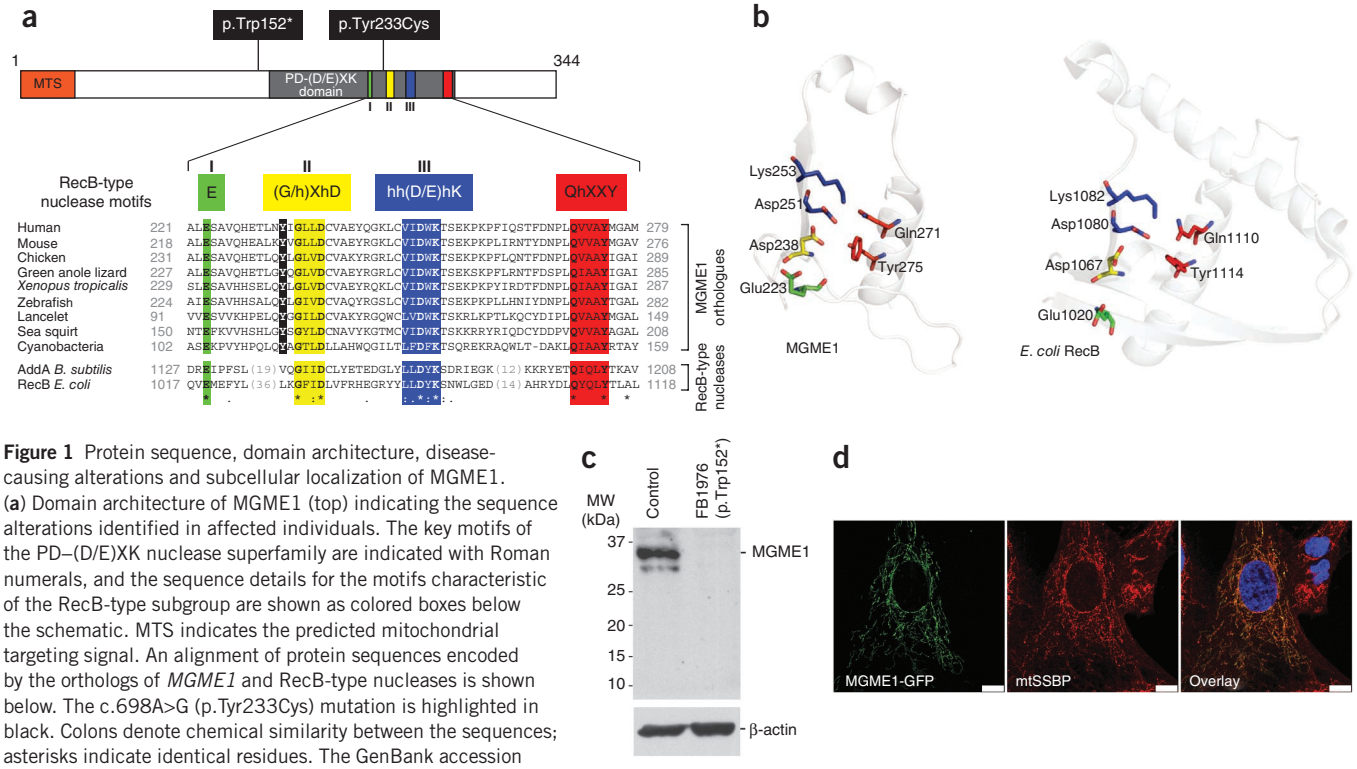

Figure 1 Protein sequence, domain architecture, disease-causing alterations and subcellular localization of MGME1. (**a**) Domain architecture of MGME1 (top) indicating the sequence alterations identified in affected individuals. The key motifs of the PD–(D/E)XK nuclease superfamily are indicated with Roman numerals, and the sequence details for the motifs characteristic of the RecB-type subgroup are shown as colored boxes below the schematic. MTS indicates the predicted mitochondrial targeting signal. An alignment of protein sequences encoded by the orthologs of *MGME1* and RecB-type nucleases is shown below. The c.698A>G (p.Tyr233Cys) mutation is highlighted in black. Colons denote chemical similarity between the sequences; asterisks indicate identical residues. The GenBank accession numbers of the sequences used in the alignment are as follows: human, NP_443097; mouse, NP_083260; chicken, XP_415017; green anole lizard, XP_003219931; *Xenopus tropicalis*, NP_001120532; zebrafish, NP_001008640; lancelet, XP_002610511; sea squirt, XP_002119404; Cyanobacteria, YP_002377694; *Bacillus subtilis* AddA, YP_004207075; *E. coli* RecB, EGB85545. (**b**) Predicted active site structural motif of MGME1 based on the known crystal structure of the homologous RecB-type nucleases. Structure prediction was made using the 3D-Jury algorithm and modeled using MODELLER software. The active site structure of *E. coli* RecB is provided for comparison. The colors used are as in **a**. (**c**) Protein blot showing the amounts of MGME1 protein in fibroblasts from P1976 (FB1976) and control fibroblasts. β-actin was used as a loading control. MW, molecular weight. (**d**) Cellular localization of the GFP-tagged variant of MGME1 (green) in human fibroblasts. mtSSBP was used as a mitochondrial marker (red). Nuclei were stained with DAPI (blue). Colocalization of the green and red signals appears yellow in digitally overlaid images. Scale bars, 10 μm.

To rescue the phenotype of the *MGME1* mutation, we transfected P1976 fibroblasts with a lentiviral wild-type *MGME1* expression construct. Expression of wild-type *MGME1* for 2 weeks substantially decreased the amount of 7S DNA, but it also caused more general mtDNA depletion (**Fig. 2c** and **Supplementary Fig. 5b**). Depletion of mtDNA was also detectable in control fibroblasts after

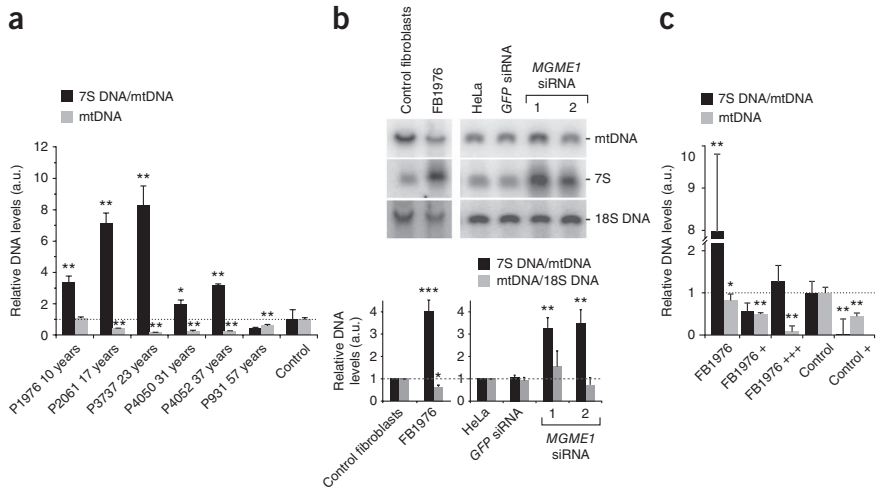

Figure 2 Loss of MGME1 leads to mtDNA depletion and higher levels of 7S DNA. (**a**) Relative mtDNA copy numbers and 7S DNA/mtDNA ratios in skeletal muscle from individuals with *MGME1* mutations. Data are shown as the averages ± s.d. from three independent quantitative PCR (qPCR) determinations and were normalized to corresponding control values, which are the averages ± s.d. from 11 skeletal muscle biopsy samples (age range of 18–33 years; mtDNA copy-number range of 8,146–11,416 molecules per nucleus). $^*P < 0.05$, $^{**}P < 0.01$; two-tailed Student's *t* test. a.u., arbitrary units. Ages at biopsy are indicated. (**b**) Total DNA from control or mutant (FB1976) fibroblasts (cell passage 15–21) and from untransfected HeLa cells or HeLa cells transfected with siRNA to *GFP* or *MGME1* for 6 d analyzed by one-dimensional Southern blotting with a radioactive probe specific for the non-coding region in human mtDNA (14,258–4,121) followed by a probe specific for 18S ribosomal DNA. Relative DNA levels were obtained by quantifying PhosphorImager scans of Southern blots using ImageQuant software and normalizing for the values obtained for control fibroblasts or untransfected HeLa cells (bottom). $^*P < 0.05$, $^{**}P < 0.01$, $^{***}P < 0.001$; two-tailed Student's *t* test; $n = 3$; error bars = 1 s.d. (**c**) Relative mtDNA copy numbers and 7S DNA/mtDNA ratios in fibroblasts from an individual with a *MGME1*-null mutation (P1976; cell passage 6–10) and a control. Where indicated, fibroblasts were transduced with low (+) or high (+++) titer of a lentivirus encoding *MGME1*. $^*P < 0.05$, $^{**}P < 0.01$; two-tailed Student's *t* test; $n = 3$; error bars = 1 s.d.

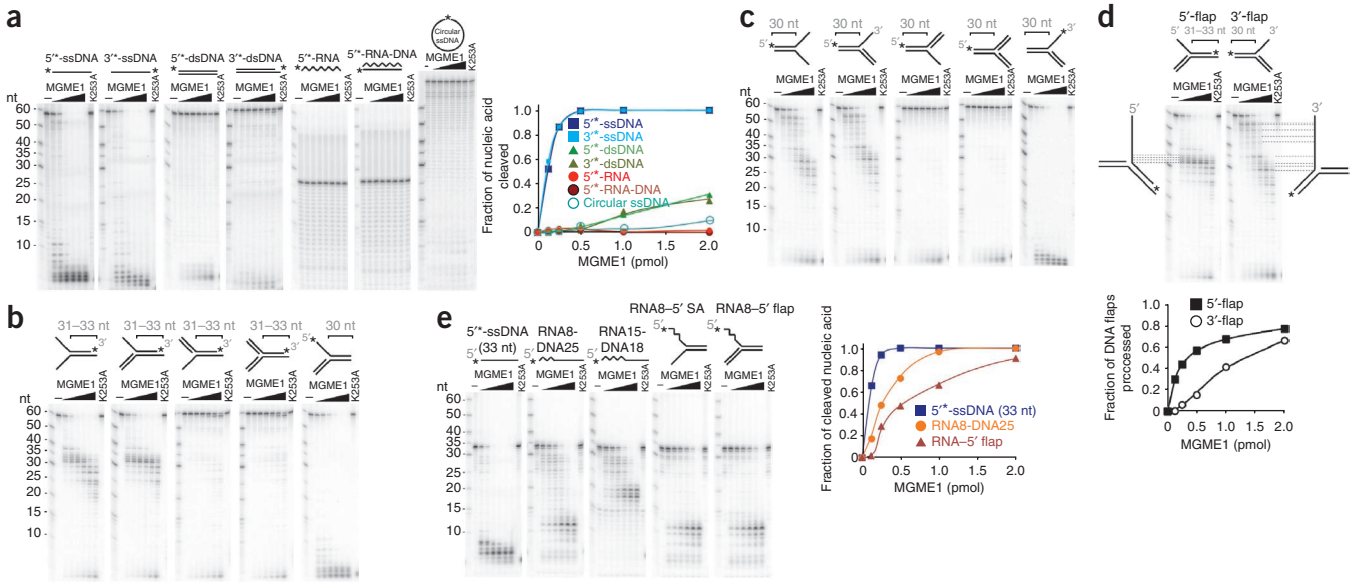

Figure 3 Characterization of the enzymatic activity of MGME1. (**a**) DNase activity of MGME1 and its preference for ssDNA versus dsDNA. Left, 1 pmol of radioactively labeled substrates (asterisks in the schematics indicate the label) were incubated for 30 min with increasing concentrations (0.125, 0.25, 0.5, 1, 2, 4 pmol) of purified MGME1 or 4 pmol of the Lys253Ala mutant (K253A). Reaction products were subjected to denaturing PAGE and autoradiography and were quantified. Right, substrate band intensity plotted against enzyme concentration. (**b**,**c**) MGME1 activity on 5′-displaced (**b**) and 3′-displaced (**c**) splayed-arm and flap-like DNA structures. Reaction conditions were the same as in **a**. (**d**) Comparison of MGME1 processing efficiency on the 5′-displaced (5′-flap) and 3′-displaced (3′-flap) flap-like DNA substrates with mapping of the radioactive products. Signal intensities of processed and partially processed reaction products were quantified and plotted as in **a**. (**e**) MGME1 activity on RNA-DNA chimeric substrates that resemble Okazaki fragments. Increasing concentrations of purified MGME1 were incubated with 5′ radioactively end-labeled RNA-DNA substrates. Numbers on the top indicate oligonucleotide lengths. SA, splayed-arm structure. Quantification of the reactions with PAGE and autoradiography is shown to the right.

lentiviral expression of wild-type *MGME1*. These findings imply that an optimal level of MGME1 is critical for the proper maintenance of the mitochondrial genome.

To investigate the enzymatic properties of MGME1, we isolated the recombinant protein from human mitochondria by affinity purification (**Supplementary Fig. 6**). MGME1 cleaved single-stranded DNA (ssDNA) but not single-stranded RNA (ssRNA) or RNA-DNA hybrids. The enzyme required free nucleic acid ends for catalysis, as it was unable to degrade circular ssDNA (**Fig. 3a**) or double-stranded DNA (dsDNA) substrates containing a nick or ssDNA gap of 12 nucleotides (**Supplementary Fig. 7**). The enzyme showed a strong preference for ssDNA over dsDNA (**Fig. 3a**). Blocking of the 5′ end but not

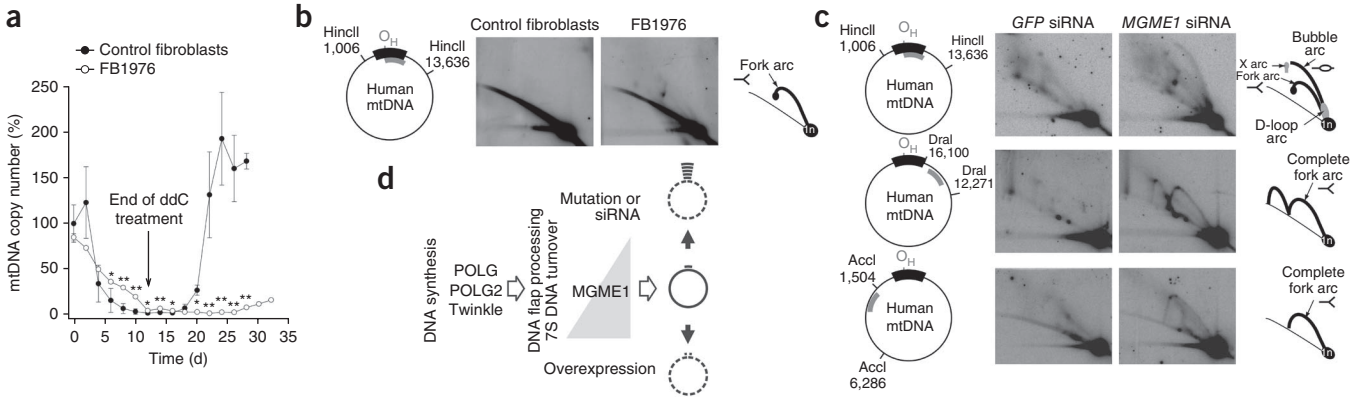

Figure 4 Perturbed mitochondrial replication in mutant fibroblasts and MGME1-depleted cells. (**a**) mtDNA copy number during induced depletion and repopulation of human control fibroblasts and MGME1-null fibroblasts (FB1976). Depletion of mtDNA was achieved by the addition of 20 μM ddC to the culture medium for 12 d. mtDNA copy numbers were determined by qPCR using the mitochondrial primers MT3922F25 and MT4036R26. Data points for FB1976 represent the mean values from three determinations ± s.d. The data for control fibroblasts are shown as the averages ± s.d. of mtDNA depletion-repopulation experiments with two separate cell lines. $*P < 0.05$, $**P < 0.01$; two-tailed Student's *t* test. (**b**,**c**) mtDNA replication in MGME1-null fibroblasts and MGME1-depleted cells. Total DNA from control or FB1976 fibroblasts (**b**) and HeLa cells transfected with siRNA to *GFP* or *MGME1* for 6 d (**c**) was subjected to two-dimensional neutral-neutral agarose gel electrophoresis followed by Southern blotting. Restriction enzymes and probes used (gray bars) are indicated to the left. The black bar indicates the non-coding region, and O_H marks the origin of H-strand replication. The interpretation based on previous work[23,28] is provided at the right. 1n, non-replicating fragment. (**d**) Schematic showing the proposed involvement of MGME1 in mtDNA maintenance. Mutation or siRNA knockdown of *MGME1* results in accumulation of replication intermediates followed by mtDNA depletion and 7S DNA accumulation (right black arrow up). In contrast, overexpression of MGME1 causes promiscuous degradation of mtDNA (including 7S DNA), resulting in mtDNA depletion (right black arrow down).

the 3′ end of ssDNA with a biotin-streptavidin moiety reduced the cleavage rate to about 10–20% of that observed for unblocked control at low enzyme concentrations (**Supplementary Fig. 8**). Recombinant MGME1 processed DNA 5′- and 3′-splayed-arm and flap-like substrates by removing the ssDNA segment but stopped at the ssDNA-dsDNA junction (**Fig. 3b**,**c**). However, the flap-like substrates with a displaced 5′ DNA end were processed more efficiently than ones with a displaced 3′ end (**Fig. 3d**). In addition, MGME1 processed RNA-DNA chimeric oligonucleotides by initiating DNA degradation at a position two to five nucleotides downstream from the RNA-DNA junction (**Fig. 3e**). Notably, the enzyme processed splayed-arm and flap-like substrates, where the displaced 5′ arm contained RNA (**Fig. 3e**). Alteration of the conserved lysine residue of the predicted PD–(D/E)XK motif III (p.Lys253Ala) completely abolished all nucleolytic activities tested (**Fig. 3** and **Supplementary Fig. 6b**). We were unable to test the enzymatic activity of the enzyme variant found in the sporadic case (p.Tyr233Cys), most likely owing to impaired folding of this variant (Online Methods and **Supplementary Fig. 6c**). These *in vitro* results confirmed the computational prediction that MGME1 is a PD–(D/E)XK-type nuclease. The requirement of nucleic acid ends with preference for the DNA 5′ end for catalysis and the ability to process DNA flap structures as well as flap structures containing RNA at the 5′ end make MGME1 a good candidate enzyme for the processing of displaced DNA containing Okazaki fragments during RNA-primed DNA synthesis on the lagging strand[19] or of DNA flaps during long-patch base excision repair[20].

To investigate the influence of the *MGME1* nonsense mutation on the ability of mtDNA to be replicated, we performed mtDNA depletion and repopulation experiments in fibroblast cultures from subject P1976. After treatment with the nucleotide analog 2′,3′-dideoxycytidine (ddC)[21], control and mutant fibroblasts developed mtDNA depletion, with mtDNA levels falling to <10% of the untreated steady-state level within 12 d of exposure (**Fig. 4a**). This depletion occurs because ddC acts both as a competitive inhibitor of mtDNA polymerase and as a terminator of nascent strand elongation[21]. After ddC withdrawal (**Fig. 4a**), mtDNA repopulation was severely impaired in *MGME1*-null cells (only 8% of control mtDNA copy number was reached after 16 d of culture without ddC). This clearly indicates perturbed mtDNA replication, similar to that observed in individuals with pathogenic *POLG* mutations[22]. Notably, the mtDNA depletion rate after exposure to ddC was considerably slower in the *MGME1*-null cells than in controls, suggesting impaired mtDNA breakdown[22].

To further examine the consequence of the *MGME1* nonsense mutation on mtDNA replication, we analyzed the pattern of mitochondrial replication intermediates in fibroblasts from affected individuals using two-dimensional agarose gel electrophoresis (2D-AGE). We observed pronounced replication stalling and accumulation of replication intermediates in the P1976 fibroblasts but not in control fibroblasts (**Fig. 4b**). These higher amounts of stalled mtDNA replication intermediates were also detected in HeLa cells subjected to siRNA targeting *MGME1*, and replication stalling was present throughout the entire mtDNA molecule (**Fig. 4c**). A similar mtDNA replication defect in 2D-AGE has been reported for mutations in *C10orf2* (Twinkle) and *POLG*[23].

In conclusion, our findings imply that mtDNA processing by MGME1 is essential for effective mtDNA synthesis. Most notably, we show that mutations affecting this mitochondrial exonuclease affect proper mtDNA maintenance (**Fig. 4d**) and are a clinically relevant cause of mtDNA disorders. Thus far, only two nuclear nucleases have also been shown to be present in mitochondria (FEN1 and DNA2)[20,24–26], and one mitochondrial enzyme (ExoG)[27] has been proposed to be involved in mtDNA flap processing. Studies on mitochondrial forms of FEN1 and DNA2 as well as ExoG have focused on their role in long-patch base excision repair in mitochondria, and nothing is known about their contribution to mtDNA replication. Although, in principle, MGME1 might have a redundant role in mtDNA repair, to our knowledge, it is the first identified mitochondrial exonuclease shown to be involved in mtDNA replication, likely through the processing of displaced DNA or RNA-DNA flap-like structures during mtDNA synthesis.

URLs. MITOMAP, http://www.mitomap.org/; HGMD (Human Gene Mutation Database), http://www.hgmd.cf.ac.uk/.

METHODS

Methods and any associated references are available in the online version of the paper.

Note: Supplementary information is available in the online version of the paper.

ACKNOWLEDGMENTS

T.J.N. and M. Minczuk are grateful to S. Wood and I. Holt for stimulating discussions during the course of this work. We are grateful to S. Beyer, K. Kappes-Horn, M. Stepien-Mering, E. Botz and R. Hellinger for technical assistance. We thank R. Wiesner (University of Cologne) for providing the TFAM antibody. This work was supported by the Medical Research Council UK (T.J.N., J.R. and M. Minczuk) and the German Bundesministerium für Bildung und Forschung (BMBF) through funding of the Systems Biology of Metabotypes grant (SysMBo 0315494A), the E-Rare project GENOMIT (01GM1207) and the German Network for mitochondrial disorders (mitoNET), including C.K., T.K. (mitoNET 01GM0862 and 01GM1113A), T.M., H.P. (mitoNET 01GM0867 and 01GM1113C) and W.S.K. (mitoNET 01GM0868). W.S.K. was funded by the Deutsche Forschungsgemeinschaft (SFB TR3 A11 and D12). V.K.M. was supported by grants from the US National Institutes of Health (GM077465 and GM097136). The financial support of Associazione Amici del Centro Dino Ferrari, University of Milan, the Telethon project GTB07001ER, the Eurobiobank project QLTR-2001-02769 and R.F. 02.187 Criobanca Automatizzata di Materiale Biologico to M.M. and M.S. are gratefully acknowledged.

AUTHOR CONTRIBUTIONS

C.K. identified, clinically characterized, collected samples and histochemically analyzed skeletal muscle biopsies from family I and the sporadic case and obtained fibroblasts from P1976. M.S., D.R., G.P.C., M. Moggio, C.M.Q. and S.D. identified, clinically characterized, collected samples and histochemically analyzed skeletal muscle biopsies from family II and obtained fibroblasts from P4050 and P4052. T.B.H., T.W., T.M.S., T.M. and H.P. performed exome sequencing and analysis of family I. S.E.C. and V.K.M. performed targeted mitochondrial exome sequencing and analysis of family II. T.J.N., G.Z. and M. Minczuk performed the computational analysis. T.J.N. analyzed protein amounts, performed subcellular localization studies, purified and characterized recombinant MGME1 and analyzed the cells with siRNA knockdown and P1976 fibroblasts. T.B.H., K.D., A.I. and H.P. performed subcellular localization and complementation experiments. S.S. performed the mtDNA repopulation experiments. V.P. performed copy-number and deletion quantification. K.H. screened PEO samples for *MGME1* mutations and identified P931. J.R. contributed to the characterization of fibroblasts from P1976. T.K. and T.M. provided samples and coordinated the German network of mitochondrial disorders. C.K., G.Z., M. Minczuk, W.S.K. and H.P. planned the project and wrote the manuscript.

COMPETING FINANCIAL INTERESTS

The authors declare no competing financial interests.

Published online at http://www.nature.com/doifinder/10.1038/ng.2501.
Reprints and permissions information is available online at http://www.nature.com/reprints/index.html.

1. Van Goethem, G. *et al.* Mutation of *POLG* is associated with progressive external ophthalmoplegia characterized by mtDNA deletions. *Nat. Genet.* **28**, 211–212 (2001).
2. Longley, M.J. *et al.* Mutant POLG2 disrupts DNA polymerase γ subunits and causes progressive external ophthalmoplegia. *Am. J. Hum. Genet.* **78**, 1026–1034 (2006).

3. Spelbrink, J.N. *et al.* Human mitochondrial DNA deletions associated with mutations in the gene encoding Twinkle, a phage T7 gene 4–like protein localized in mitochondria. *Nat. Genet.* **28**, 223–231 (2001).
4. Nishino, I., Spinazzola, A. & Hirano, M. Thymidine phosphorylase gene mutations in MNGIE, a human mitochondrial disorder. *Science* **283**, 689–692 (1999).
5. Kaukonen, J. *et al.* Role of adenine nucleotide translocator 1 in mtDNA maintenance. *Science* **289**, 782–785 (2000).
6. Mandel, H. *et al.* The deoxyguanosine kinase gene is mutated in individuals with depleted hepatocerebral mitochondrial DNA. *Nat. Genet.* **29**, 337–341 (2001).
7. Saada, A. *et al.* Mutant mitochondrial thymidine kinase in mitochondrial DNA depletion myopathy. *Nat. Genet.* **29**, 342–344 (2001).
8. Elpeleg, O. *et al.* Deficiency of the ADP-forming succinyl-CoA synthase activity is associated with encephalomyopathy and mitochondrial DNA depletion. *Am. J. Hum. Genet.* **76**, 1081–1086 (2005).
9. Spinazzola, A. *et al. MPV17* encodes an inner mitochondrial membrane protein and is mutated in infantile hepatic mitochondrial DNA depletion. *Nat. Genet.* **38**, 570–575 (2006).
10. Bourdon, A. *et al.* Mutation of *RRM2B*, encoding p53-controlled ribonucleotide reductase (p53R2), causes severe mitochondrial DNA depletion. *Nat. Genet.* **39**, 776–780 (2007).
11. Ostergaard, E. *et al.* Deficiency of the α subunit of succinate–coenzyme A ligase causes fatal infantile lactic acidosis with mitochondrial DNA depletion. *Am. J. Hum. Genet.* **81**, 383–387 (2007).
12. Haack, T.B. *et al.* Molecular diagnosis in mitochondrial complex I deficiency using exome sequencing. *J. Med. Genet.* **49**, 277–283 (2012).
13. Elstner, M. *et al.* MitoP2: an integrative tool for the analysis of the mitochondrial proteome. *Mol. Biotechnol.* **40**, 306–315 (2008).
14. Calvo, S.E. *et al.* Molecular diagnosis of infantile mitochondrial disease with targeted next-generation sequencing. *Sci. Transl. Med.* **4**, 118ra10 (2012).
15. Pagliarini, D.J. *et al.* A mitochondrial protein compendium elucidates complex I disease biology. *Cell* **134**, 112–123 (2008).
16. Steczkiewicz, K. *et al.* Sequence, structure and functional diversity of PD-(D/E)XK phosphodiesterase superfamily. *Nucleic Acids Res.* **40**, 7016–7045 (2012).
17. Aravind, L. *et al.* Holliday junction resolvases and related nucleases: identification of new families, phyletic distribution and evolutionary trajectories. *Nucleic Acids Res.* **28**, 3417–3432 (2000).
18. Singleton, M.R. *et al.* Crystal structure of RecBCD enzyme reveals a machine for processing DNA breaks. *Nature* **432**, 187–193 (2004).
19. Holt, I.J. *et al.* Coupled leading- and lagging-strand synthesis of mammalian mitochondrial DNA. *Cell* **100**, 515–524 (2000).
20. Liu, P. *et al.* Removal of oxidative DNA damage via FEN1-dependent long-patch base excision repair in human cell mitochondria. *Mol. Cell. Biol.* **28**, 4975–4987 (2008).
21. Brown, T.A. & Clayton, D.A. Release of replication termination controls mitochondrial DNA copy number after depletion with 2′,3′-dideoxycytidine. *Nucleic Acids Res.* **30**, 2004–2010 (2002).
22. Stewart, J.D. *et al. POLG* mutations cause decreased mitochondrial DNA repopulation rates following induced depletion in human fibroblasts. *Biochim. Biophys. Acta* **1812**, 321–325 (2011).
23. Wanrooij, S. *et al.* Expression of catalytic mutants of the mtDNA helicase Twinkle and polymerase POLG causes distinct replication stalling phenotypes. *Nucleic Acids Res.* **35**, 3238–3251 (2007).
24. Copeland, W.C. & Longley, M.J. DNA2 resolves expanding flap in mitochondrial base excision repair. *Mol. Cell* **32**, 457–458 (2008).
25. Zheng, L. *et al.* Human DNA2 is a mitochondrial nuclease/helicase for efficient processing of DNA replication and repair intermediates. *Mol. Cell* **32**, 325–336 (2008).
26. Duxin, J.P. *et al.* Human Dna2 is a nuclear and mitochondrial DNA maintenance protein. *Mol. Cell. Biol.* **29**, 4274–4282 (2009).
27. Tann, A.W. *et al.* Apoptosis induced by persistent single-strand breaks in mitochondrial genome: critical role of EXOG (5′-EXO/endonuclease) in their repair. *J. Biol. Chem.* **286**, 31975–31983 (2011).
28. Pohjoismäki, J.L. *et al.* Mammalian mitochondrial DNA replication intermediates are essentially duplex but contain extensive tracts of RNA/DNA hybrid. *J. Mol. Biol.* **397**, 1144–1155 (2010).

ONLINE METHODS

Mutation screening. Exome sequencing of the index subject of family I (P1976) was performed on a Genome Analyzer IIx system (Illumina) after in-solution enrichment of exonic sequences (SureSelect Human All Exon 38Mb kit, Agilent). The sample was sequenced using two lanes of a flow cell as 54-bp paired-end runs. Read alignment was performed with Burrows-Wheeler Aligner (BWA, version 0.5.8) to the human genome assembly hg19. Single-nucleotide variants and small insertions and deletions were detected with SAMtools (v 0.1.7). Variant annotation was performed with custom scripts. Considering the context of a mitochondrial disorder, we focused on genes encoding proteins with confirmed or predicted mitochondrial localization corresponding to a MitoP2 score of >0.5 (ref. 13). Sequence analysis by Sanger sequencing confirmed the presence of the c.456G>A mutation in *C20orf72* in the homozygous state in all three affected siblings from family I.

The homozygous nonsense mutation (c.456G>A, p.Trp152*) in subject P4052 from family II was detected by a MitoExome sequencing approach described previously[15]. Briefly, DNA was extracted from blood, and hybrid selection (Agilent SureSelect) was used to select for the mtDNA and coding exons of over 1,000 nuclear genes associated with mitochondrial function[15], which were sequenced by Illumina HiSeq with paired 76-bp reads. Reads were aligned to the reference human genome assembly hg19, and variants were detected using the Genome Analysis Toolkit[29]. All variants previously associated with disease (MITOMAP and HGMD) were prioritized as were all rare variants predicted to be deleterious and consistent with a recessive mode of pathogenesis[29]. The homozygous variant c.456G>A (p.Trp152*) in *C20orf72* was the only candidate mutation meeting these stringent prioritization criteria.

The homozygous c.698A>G (p.Tyr233Cys) *C20orf72* mutation in subject P931 was detected in a screening of 50 German individuals with PEO by Sanger sequencing. The study was approved by the Ethical Committees of the Universities of Bonn (186/09) and Milan and the Technical University Munich, and written informed consent was obtained from all subjects.

qPCR. The copy numbers of mtDNA were determined by qPCR essentially as described previously[30]. Briefly, a segment of the mtDNA outside the 7S region was amplified using primers MT3922F25 and MT4036R26 (first number, 5′ nucleotide of primer; second number, length of primer; F, forward primer; R, reverse primer; numbering according to reference sequence NC_012920). Primers MT16520F24 and MT35R24 were used together with TaqMan probe MT16557F25 to amplify a short segment inside the 7S region of the mtDNA. C_T values were defined at the inflection points of fitted sigmoid curves (four-parameter Chapman curves) and were compared to those of the single-copy nuclear gene *KCNJ10* amplified by primers KIR835F19 and KIR903R19 and TaqMan probe KIR857F27 (numbering according to sequence U52155). Relative 7S/mtDNA ratios were calculated by subtracting copy numbers outside 7S from those inside 7S, dividing by copy numbers outside 7S and subsequently normalizing to the control value. Reactions were performed on a MyiQ qPCR system (Bio-Rad) using either TaqMan probes or iQ SYBR Green Supermix (Bio-Rad) under the following conditions: 95 °C for 3 min and 45 cycles of 95 °C for 15 s and 60 °C for 1 min. Primer sequences are listed in **Supplementary Table 5**.

Detection of mtDNA deletions. Large-scale deletions of the mitochondrial genome were detected by long-range PCR using either primer pair MT5462F28 and MT45R22 or the primer pair MT15974F23 and MT15623R20 (**Supplementary Table 5**). For amplification, TaKaRa LA Taq Hot Start DNA polymerase (Takara Bio) was used under the following conditions: 95 °C for 2.5 min, 10 cycles of 92 °C for 20 s and 68 °C for 14 min, 20 cycles of 92 °C for 25 s and 68 °C for 16 min, and 72 °C for 10 min. To quantify deletion levels, a single-molecule PCR approach was used as described previously[30]. Briefly, single mtDNA deletions were amplified using the same conditions as in long-range PCR, but in 42 cycles of PCR. To estimate the amounts of total mtDNA, primers MT16520F24 and MT4833R24 were used. Total template DNA was diluted stepwise to the point where only some of the multiple identical reactions resulted in amplification products (ideally less than 50%). It is reasonable to assume that, under these conditions, each positive reaction originated from a single mtDNA molecule or a single deleted mtDNA molecule dividing the degree of dilution for single mtDNA molecules by the degree of dilution for single deleted mtDNA molecules (for example, 6 positive reactions out of 15 at dilution 10^{-5} for total mtDNA and 3 positive reactions out of 15 at dilution 10^{-3} for deleted mtDNA gives a deletion ratio of 5×10^{-3}).

Cell culture, transduction and transfection. HeLa cells were cultured in DMEM (Gibco) supplemented with 10% FCS (Thermo Scientific), 10 U/ml penicillin and 10 µg/ml streptomycin (Gibco). Fibroblast cell lines were maintained in high-glucose DMEM (Invitrogen) supplemented with 10% FBS (Invitrogen), 200 µM uridine (Sigma) and 1% penicillin-streptomycin (Invitrogen) at 37 °C in a humidified atmosphere of 5% CO_2.

The *C20orf72* ORF was cloned into the lentiviral expression vector pLENTI6.3. The pLenti6.3/V5-TOPO vector system (Invitrogen) was used for the lentivirus-mediated expression of wild-type cDNA in skin fibroblast cell lines[31]. Transfected HEK 293 cells were maintained in DMEM containing 10% tetracycline-free FCS (Biochrom AG), 10 U/ml penicillin and 10 µg/ml streptomycin (Gibco), 50 µg/ml hygromycin (Invitrogen) and 15 µg/ml blasticidin (Invivogen). For siRNA experiments, 100,000 cells were transfected with siRNA against *MGME1* or negative control (Invitrogen Stealth) using Lipofectamine RNAiMAX (Invitrogen) for 3 d and then transfected again for a further 3 d. siRNA sequences are given in **Supplementary Table 5**.

Protein purification. The full-length cDNA clone for *MGME1* was obtained from MRC Geneservice and cloned in-frame with a sequence encoding a Flag-Strep2 tag into the expression vector pcDNA5/FRT/TO (Invitrogen). cDNA clones for the Tyr233Cys and Lys253Ala variants of MGME1 were created by oligonucleotide-directed mutagenesis (primer sequences are given in **Supplementary Table 5**). The constructs encoding wild-type, Tyr233Cys and Lys253Ala MGME1 were transfected into HEK Flp-In T-Rex 293 cells (Invitrogen) using Cell Line Nucleofector (Lonza), applying program A-23. Transfected cells were induced to express recombinant MGME1 or its mutants with 50 ng/ml doxycycline for 48 h, after which time mitochondria were isolated by hypotonic lysis and differential centrifugation, as described previously[32]. Recombinant MGME1 protein was isolated using a gravity-flow Strep-Tactin column (IBA) as described previously[32]. To assess the purity of the recombinant enzymes, Strep-Tactin–purified proteins were separated by SDS-PAGE and stained with Coomassie, and all protein bands were excised from the gels and identified by mass spectrometry. Typically, for the wild-type and Lys253Ala variants, the procedure yielded ~150 µg of recombinant enzyme that was ~95% pure, starting from 4–4.5 g of cells (**Supplementary Fig. 6a**,**b**). Under the same conditions, the Tyr233Cys variant gave only about 1/30 of this yield, and preparations were contaminated (~90%) with the mitochondrial chaperone HSP70, suggestive of impaired folding of the recombinant Tyr233Cys protein (**Supplementary Fig. 6c**).

***In vitro* nuclease assays.** Labeled substrates (1 nmol) were incubated with the indicated amounts of purified MGME1 protein in a reaction buffer containing 10 mM Tris, pH 7.6, 20 mM $MgCl_2$, 1 mM DTT and 0.1 mg/ml BSA at 37 °C for 30 min. Reactions were then snap frozen on dry ice and separated on 10% denaturing polyacrylamide gels, and gels were dried and imaged using a PhosphorImager (GE Healthcare). For streptavidin end blocking of biotinylated oligonucleotides, reactions also contained 15 mg/ml streptavidin (NEB).

DNA isolation, gel separation and hybridization. For one-dimensional gels, 3 µg of total genomic DNA was digested according to the manufacturer's instructions (NEB), separated on 0.6% agarose gels and blotted overnight onto nylon membrane (GE Magnaprobe). Membranes were hybridized with appropriate radio-labeled probes overnight at 65 °C in 7% SDS and 0.25 M sodium phosphate buffer (pH 7.6), washed with 1× SSC (150 mM sodium chloride and 15 mM sodium citrate, pH 7.0) with 0.1% SDS three times for 20 min at 65 °C and imaged using a PhosphorImager. For two-dimensional gels, total DNA was isolated from cells by sequential phenol-chloroform extraction according to established protocols[33]. Resulting DNA (10–20 µg) was digested according to the manufacturer's instructions (NEB) and separated on agarose gels according to protocols described in detail elsewhere[33]. Gels were then blotted and hybridized as described for one-dimensional gels and were washed with 1× SSC three times for 20 min and then with 1× SSC with 0.1% SDS three times for 20 min. The primer sequences used to produce the probes are given in **Supplementary Table 5**.

Antibodies. Protein blotting was performed on cell lysates and cell fractions using primary antibodies to MGME1 (Sigma, HPA040913; 1:500 dilution),

doi:10.1038/ng.2501

β-actin (Sigma, A2228; 1:100,000 dilution), TFAM (R. Wiesner, University of Cologne; 1:40,000 dilution), Histone H4 (Abcam, ab10158; 1:5,000 dilution), GAPDH (Abcam, ab9482; 1:1,000 dilution) and TOM20 (Santa Cruz Biotechnology, sc-11415; 1:1,000 dilution). Secondary antibodies used were horseradish peroxidase (HRP)-conjugated goat antibodies to rabbit (Promega, W401B; 1:2,000 dilution) and mouse (Promega, W402B, 1:2,000 dilution).

29. McKenna, A. *et al.* The Genome Analysis Toolkit: a MapReduce framework for analyzing next-generation DNA sequencing data. *Genome Res.* **20**, 1297–1303 (2010).
30. Zsurka, G. *et al.* Clonally expanded mitochondrial DNA mutations in epileptic individuals with mutated DNA polymerase γ. *J. Neuropathol. Exp. Neurol.* **67**, 857–866 (2008).
31. Danhauser, K. *et al.* Cellular rescue-assay aids verification of causative DNA-variants in mitochondrial complex I deficiency. *Mol. Genet. Metab.* **103**, 161–166 (2011).
32. Rorbach, J. *et al.* PDE12 removes mitochondrial RNA poly(A) tails and controls translation in human mitochondria. *Nucleic Acids Res.* **39**, 7750–7763 (2011).
33. Reyes, A. *et al.* Analysis of replicating mitochondrial DNA by two-dimensional agarose gel electrophoresis. *Methods Mol. Biol.* **372**, 219–232 (2007).